1   **Reviewing Global Estimates of Surface Reactive Nitrogen Concentration and**

2   **Deposition Using Satellite Observation**

3   Lei Liu [a, *], Xiuying Zhang [b], Wen Xu [c], Xuejun Liu [c], Xuehe Lu [b], Jing Wei [d, e], Yi Li [f],

4   Yuyu Yang [a], Zhen Wang [b], Anthony Y. H. Wong [g]

5   [a] College of Earth and Environmental Sciences, Lanzhou University, Lanzhou 730000,

6   China

7   [b] International Institute for Earth System Science, Nanjing University, Nanjing,

8   210023, China

9   [c] College of Resources and Environmental Sciences, National Academy of

10   Agriculture Green Development, China Agricultural University, Beijing, 100193,

11   China

12   [d] State Key Laboratory of Remote Sensing Science, College of Global Change and

13   Earth System Science, Beijing Normal University, Beijing, China

14   [e] Department of Atmospheric and Oceanic Science, Earth System Science

15   Interdisciplinary Center, University of Maryland, College Park, MD, USA

16   [f] Chief Technology Officer SailBri Cooper Inc., Beaverton OR, 97008, USA

17   [g] Department of Earth and Environment, Boston University, Boston, MA 02215, USA

18   * Correspondence to Lei Liu (liuleigeo@lzu.edu.cn).

19   **Abstract**

20   Since the industrial revolution, human activities have dramatically changed the

21   nitrogen (N) cycle in natural systems. Anthropogenic emissions of reactive nitrogen

22   (N_r) can return to the earth's surface through atmospheric N_r deposition. Increased N_r

23   deposition may improve ecosystem productivity. However, excessive N_r deposition

24   can cause a series of negative effects on ecosystem health, biodiversity, soil, and

25   water. Thus, accurate estimations of N_r deposition are necessary for evaluating its

26 environmental impacts. The United States, Canada and Europe have successively

27 launched a number of satellites with sensors that allow retrieval of atmospheric NO_2

28 and NH_3 column density, and therefore estimation of surface N_r concentration and

29 deposition at an unprecedented spatiotemporal scale. Atmosphere NH_3 column can be

30 retrieved from atmospheric infra-red emission measured by IASI, AIRS, CrIS or TES,

31 while atmospheric NO_2 column can be retrieved from reflected solar radiation

32 measured by GOME, GOME-2, SCIAMACHY, OMI, TEMPO, Sentinel and GEMS.

33 In recent years, scientists attempted to estimate surface N_r concentration and

34 deposition using satellite retrieval of atmospheric NO_2 and NH_3 columns. In this study,

35 we give a thorough review on recent advances of estimating surface N_r concentration

36 and deposition using the satellite retrievals of NO_2 and NH_3, present a framework of

37 using satellite data to estimate surface N_r concentration and deposition based on

38 recent works, and summarize the existing challenges for estimating surface N_r

39 concentration and deposition using the satellite-based methods. We believe that

40 exploiting satellite data to estimate N_r deposition has a broad and promising prospect.

41 **Keywords**

42 Nitrogen deposition; Satellite retrieval; Surface concentration; Oxidized and reduced

43 N_r

44 **1. Introduction**

45 Nitrogen (N) exists in three forms in the environment including reactive nitrogen (N_r),

46 organic nitrogen (ON) and nitrogen gas (N_2) (Canfield et al., 2010). N_2 is the main

47 component of air, accounting for 78% of the total volume of air, but it cannot be

48 directly used by most plants. N_r (such as NO_3^- and NH_4^+) is the main form of N that

49 can be directly used by most plants, but the content of N_r in nature is much lower

50 compared with ON and N_2 (Vitousek et al., 1997;Nicolas and Galloway, 2008). The

Atmospheric
Chemistry
and Physics
Discussions

51 supply of N_r is essential for all life forms and contributes to the increase in

52 agricultural production, thus providing sufficient food for the growing global

53 population (Galloway et al., 2008;David et al., 2013;Galloway et al., 2004b;Erisman

54 et al., 2008). Before the industrial revolution, N_r mainly came from natural sources

55 such as biological N fixation, lightning and volcanic eruption (Galloway et al., 2004a).

56 Since the industrial revolution, human activities (e.g. agricultural development,

57 combustion of mineral energy) have greatly perturbed the N cycle in natural systems

58 (Canfield et al., 2010;Kim et al., 2014;Lamarque et al., 2005).

59 N_r (NO_x and NH_3) emitted to the atmosphere will return to the earth surface through

60 atmospheric deposition (Liu et al., 2011). Atmospheric N_r deposition refers to the

61 process in which N_r are removed from the atmosphere, including wet (rain and snow)

62 and dry (gravitational settling, atmospheric turbulence, etc.) deposition (Xu et al.,

63 2015;Zhang et al., 2012;Pan et al., 2012). The input of N_r over terrestrial natural

64 ecosystems primarily comes from the N_r deposition (Shen et al., 2013;Sutton et al.,

65 2001;Larssen et al., 2011). In the short term, atmospheric N_r deposition can increase

66 the N_r input to ecosystems, which promotes plant growth and enhances ecosystem

67 productivity (Erisman et al., 2008;Sutton et al., 2013). However, excessive

68 atmospheric N_r deposition also causes a series of environmental problems (Liu et al.,

69 2017d). Due to the low efficiency of agricultural N application, plenty of N_r is lost

70 through runoff, leaching and volatilization, causing serious environmental pollution.

71 Excessive N_r deposition may aggravate the plant's susceptibility to drought or frost,

72 reduce the resistance of plant to pathogens or pests, and further affect the physiology

73 and biomass distribution of vegetation (ratio of roots, stems and leaves) (Stevens et al.,

74 2004;Nadelhoffer et al., 1999;Bobbink et al., 2010;Janssens et al., 2010). Excessive

75 N_r leads to eutrophication and related algal blooms over aquatic ecosystems, reducing

Atmospheric
Chemistry
and Physics
Discussions

76   water biodiversity (Paerl et al., 2014), while excessive N_r in drinking water also poses

77   a threat to human health (Zhao et al., 2013). Therefore, monitoring and estimation of

78   surface N_r concentration and deposition on the global scale are of great importance

79   and urgency.

80   The methods of estimating atmospheric N_r deposition can be divided into three

81   categories: ground-based monitoring, atmospheric chemical transport modeling

82   (ACTM) and satellite-based estimation. Ground-based monitoring is considered to be

83   the most accurate quantitative method, which can effectively reflect the N_r deposition

84   in local areas. ACTM can simulate the processes of N_r chemical reaction, transport,

85   and deposition, as well as the vertical distribution of N_r. Satellite-based estimation

86   establishes empirical, physical or semi-empirical models by connecting the

87   ground-based N_r concentrations and deposition with satellite-derived N_r concentration.

88   This study focuses on reviewing the recent development of satellite-based methods to

89   estimate N_r deposition. We firstly give a brief introduction to the progress of

90   ground-based monitoring, ACTM-based methods, and then present a detailed

91   framework of using satellite observation to estimate dry and wet N_r deposition

92   (including both oxidized and reduced N_r). Next, we review the recent advances of the

93   satellite-based methods of estimating N_r deposition. Finally, we discuss the remaining

94   challenges for estimating surface N_r concentration and deposition using satellite

95   observation.

96   **2.1 Methods for Estimating Surface N_r Concentration and Deposition**

97   **2.1.1 Ground-based Monitoring**

98   Ground-based monitoring of N_r deposition can be divided into two parts: wet and dry

99   N_r deposition monitoring. Since the 1970s, there have been large-scale monitoring

100 networks focusing on the wet N_r deposition. The main large-scale regional monitoring

101   networks include Canadian Air and Precipitation Monitoring Network (CAPMoN),

102   Acid Deposition Monitoring Network in East Asia (EANET), European Monitoring

103   and Evaluation Program (EMEP), United States National Atmospheric Deposition

104   Program (NADP), World Meteorological Organization Global Atmosphere Watch

105   Precipitation Chemistry Program, and Nationwide Nitrogen Deposition Monitoring

106   Network in China (NNDMN) (Tan et al., 2018;Vet et al., 2014). The detailed

107   scientific objectives of the wet N_r deposition observation networks vary, but most of

108   the observation networks mainly concentrate on the spatiotemporal variation of wet

109   deposition of ions including N_r compounds, the long-term trends of ions in

110   precipitation, and the evaluation of ACTMs.

111   Compared with wet N_r deposition monitoring, dry N_r deposition monitoring started

112   late, due to the limitation of monitoring technology since it is more difficult to be

113   quantified (affected greatly by surface roughness, air humidity, climate and other

114   environmental factors) (Liu et al., 2017c). Dry N_r deposition observation networks

115   include US ammonia monitoring network (AMoN), CAPMoN, EANET and EMEP.

116   The monitoring methods of dry N_r deposition are mainly divided into direct

117   monitoring (such as dynamic chambers) and indirect monitoring (such as inferential

118   methods). The inferential model is widely applied in ground-based monitoring

119   networks (such as EANET and NNDMN), mainly because this method is more

120   practical and simpler. In inferential models, dry deposition is divided into two parts:

121   surface N_r concentrations and the deposition velocity (V_d) of N_r (Nowlan et al., 2014).

122   V_d can be estimated by meteorology, land use types of underlying surface as well as

123   the characteristics of each N_r component itself using resistance models (Nemitz et al.,

124   2001). Thus, dry N_r deposition monitoring networks only need to focus on the

125   quantification of surface concentration of individual N_r components. The N_r

126 components in the atmosphere are very complex, including N_2O_5, HONO, NH_3, NO_2,

127 HNO_3 and particulate NH_4^+ and NO_3^-. Most monitoring networks include the major

128 N_r species such as gaseous NH_3, NO_2, HNO_3 and the particles of NH_4^+ and NO_3^-.

129 Effort of ground-based N_r deposition monitoring mostly concentrates on wet N_r

130 deposition, while observations of dry N_r deposition are relatively scarce especially for

131 surface HNO_3 and NH_4^+ and NO_3^-. Second, most observation networks focus on a few

132 years or a certain period of time, leading to the lack of long-term continuously

133 monitoring on both wet and dry N_r deposition. More importantly, the global N_r

134 deposition monitoring network has not been established, and the sampling standards

135 in different regions are not unified. These outline the potential room for improvement

136 of ground-based N_r deposition monitoring.

137 **2.1.2 ACTM Simulation**

138 An ACTM can simulate N_r deposition at regional or global scales through explicitly

139 representing the physical and chemical processes of atmospheric N_r components

140 (Zhao et al., 2017;Zhang et al., 2012). Wet N_r deposition flux is parameterized as

141 in-cloud, under-cloud and precipitation scavenging (Amos et al., 2012;Levine and

142 Schwartz, 1982;Liu et al., 2001;Mari et al., 2000), while dry deposition flux can be

143 obtained as the product of surface N_r concentration and V_d, which is typically

144 parameterized as a network of resistances (Wesely and Hicks, 1977). Based on the

145 integrated results of 11 models of HTAP (hemispheric transport of air pollution), Tian

146 et al. found that about 76%-83% of the ACTM's simulation results were ±50% of the

147 monitoring values, and the modeling results underestimated the wet deposition of

148 NH_4^+ and NO_3^- over Europe and East Asia, and overestimated the wet deposition of

149 NO_3^- over the eastern US. Though regional ACTMs can be configured at very high

150 horizontal resolution (e.g., 1×1 km^2) (Kuik et al., 2016), the horizontal resolution of

151   global ACTMs are relatively coarse ($1°×1°$-$5°×4°$) (Williams et al., 2017), which

152   cannot indicate the local pattern of N_r deposition. On the other hand, the N_r emission

153   inventory used to drive an ACTM is highly uncertain, with the uncertainty of the NO_x

154   emission at about ±30-40%, and that of NH_3 emission at about ±30-80% (Zhang et al.,

155   2009;Cao et al., 2011).

156   **2.1.3 Satellite-based Estimation of Surface N_r Concentration and Deposition**

157   Satellite observation has wide spatial coverages and high resolution, and is

158   spatiotemporally continuous. Atmospheric NO_2 and NH_3 columns can be derived

159   from satellite measurements with relatively high accuracy (Van Damme et al.,

160   2014a;Boersma et al., 2011), providing a new perspective about atmospheric N_r

161   abundance.

162   Satellite instruments that can monitor NO_2 in the atmosphere include GOME (Global

163   Ozone Monitoring Experience), SCIAMACHY (SCanning Imaging Absorption

164   SpectroMeter for Atmospheric ChartographY), OMI (Ozone Monitoring Instrument),

165   GOME-2 (Global Ozone Monitoring Experience-2). Some scholars applied satellite

166   NO_2 columns to estimate the surface NO_2 concentration, and then dry NO_2 deposition

167   by combining the surface NO_2 concentration and modeled V_d. Cheng et al. (Cheng et

168   al., 2013) established a statistical model to estimate the surface NO_2 concentration

169   based on the SCIAMACHY NO_2 columns, and then estimated the dry deposition of

170   NO_2 over eastern China. This method by Cheng et al. (Cheng et al., 2013) using the

171   simple linear model did not consider the vertical profiles of NO_2. Lu et al. (Lu et al.,

172   2013) established a multivariate linear regression model based on the SCIAMACHY

173   and GOME NO_2 columns, meteorological data and ground-based monitoring N_r

174   deposition, and then estimated the global total N_r deposition. Lu et al. (Lu et al., 2013)

175   could not distinguish the contribution of dry and wet N_r deposition using the

176   multivariate linear regression model. Jia et al. (Jia et al., 2016) established a simple

177   linear regression model based on OMI tropospheric NO_2 column and ground-based

178   surface N_r concentration, and then estimated the total amounts of dry N_r deposition.

179   Jia et al. (Jia et al., 2016) used OMI tropospheric NO_2 column to estimate the dry

180   deposition of reduced N_r deposition (NH_3 and NH_4^+), which could also bring great

181   errors since the OMI NO_2 column could not indicate the NH_3 emission. These studies

182   highlight the problem of using only NO_2 columns to derive total N_r deposition, that

183   NO_2 columns give us highly limited information about the abundance of reduced N_r

184   (NH_3 and NH_4^+).

185   Lamsal et al. (Lamsal et al., 2008) first used the relationship between the NO_2 column

186   and surface NO_2 concentration at the bottom layer simulated by an ACTM to convert

187   OMI NO_2 column to surface NO_2 concentration. A series of works (Lamsal et al.,

188   2013;Nowlan et al., 2014;Kharol et al., 2018) have effectively estimated regional and

189   global surface NO_2 concentration using satellite NO_2 column combining with

190   ACTM-derived relationship between the NO_2 column and surface NO_2 concentration

191   simulated. It is worth mentioning that Nowlan et al. (Nowlan et al., 2014) applied

192   OMI NO_2 column to obtain the global dry NO_2 deposition during 2005-2007 for the

193   first time. However, using satellite NO_2 column and ACTM-derived relationship

194   between the NO_2 column and surface NO_2 concentration may lead to an

195   underestimation of surface NO_2 concentration. Kharol et al. (Kharol et al., 2015)

196   found that the satellite-derived surface NO_2 concentration using the above method is

197   only half of the observed values. To resolve such potential underestimation, Larkin et

198   al. (Larkin et al., 2017) established a statistical relationship between the

199   satellite-derived and ground measured surface NO_2 concentration, and then calibrated

200   the satellite-derived surface NO_2 concentration using the established relationship.

Atmospheric
Chemistry
and Physics
Discussions
Open Access
EGU

201 Some researchers also estimated other N_r components (such as particulate NO_3^-)

202 based on satellite NO_2 column. Based on the linear model between NO_2, NO_3^-, HNO_3

203 obtained by ground-based measurements, Jia et al. (Jia et al., 2016) calculated the

204 surface NO_3^- and HNO_3 concentration using satellite-derived surface NO_2

205 concentration and their relationship. Geddes et al. (Geddes and Martin, 2017)

206 reconstructed the NO_x emission data by using the satellite NO_2 column, and then

207 estimated the global NO_x deposition by an ACTM, but the spatial resolution of global

208 NO_x deposition remains low ($2°\times2.5°$), failing to exploit the higher resolution of

209 satellite observation.

210 Comparing with NO_2, the development of satellite NH_3 monitoring is relatively late.

211 Atmospheric NH_3 was first detected by the TES in Beijing and Los Angeles (Beer et

212 al., 2008). The IASI sensor also detected atmospheric NH_3 from a biomass burning

213 event in Greece (Coheur et al., 2009). Subsequently, many scholars began to develop

214 more reliable satellite NH_3 column retrievals (Whitburn et al., 2016;Van Damme et al.,

215 2014a), validate the satellite-retrieved NH_3 column with the ground-based observation

216 (Van Damme et al., 2014a;Dammers et al., 2016;Li et al., 2017), and compare the

217 satellite NH_3 column with the aircraft measured NH_3 column (Van Damme et al.,

218 2014b;Whitburn et al., 2016). In recent years, some scholars have carried out the

219 works of estimating surface NH_3 concentration based on satellite NH_3 column. Liu et

220 al. (Liu et al., 2017b) obtained the satellite-derived surface NH_3 concentration in

221 China based on the IASI NH_3 column coupled with an ACTM, and deepened the

222 understanding of the spatial pattern of surface NH_3 concentration in China. Similarly,

223 Graaf et al. (Van der Graaf et al., 2018) carried out the relevant work in Europe based

224 on the IASI NH_3 column coupled with an ACTM, and estimated the dry NH_3

225 deposition in West Europe. Jia et al. (Jia et al., 2016) first constructed the linear model

226   between surface NO_2 and NH_4^+ concentration based on ground monitoring data, and

227   then calculated the NH_4^+ concentration using satellite-derived surface NO_2

228   concentration and their relationship. However, as the emission sources of NO_x

229   (mainly from transportation and energy sectors) and NH_3 (mainly from agricultural

230   sector) are different (Hoesly et al., 2018), the linear model between surface NO_2 and

231   NH_4^+ concentration may lead to large uncertainties in estimating the global NH_4^+

232   concentration. There is still no report about the satellite-derived dry and wet reduced

233   N_r deposition using satellite NH_3 column at a global scale. As reduced N_r plays an

234   important role in total N_r deposition, satellite NH_3 should be better utilized to help

235   estimate reduced N_r deposition.

236   **2.1.4 Problems in Estimating Global N_r Deposition**

237   The spatial coverage of ground monitoring sites focusing on N_r deposition is still not

238   adequate, and the monitoring standards and specifications in different regions of the

239   world are not consistent, presenting a barrier to integrating different regional

240   monitoring data. Large uncertainties exist in N_r emission inventory used to drive the

241   ACTMs, and the spatial resolution of the modeled N_r deposition by ACTMs is coarse.

242   Using satellite monitoring data to estimate surface N_r concentration and deposition is

243   still in its infancy, especially for reduced N_r.

244   Some scholars tried to use satellite NO_2 and NH_3 column to estimate the surface N_r

245   concentration and dry N_r deposition. However, there are relatively few studies on

246   estimating wet N_r deposition. In addition, the development of satellite monitoring for

247   NH_3 in the atmosphere is relatively late (compared with NO_2). At present, IASI NH_3

248   data have been widely used, while the effective measurements of TES are less than

249   IASI; CrIS and AIRS NH_3 column products are still under development. There are

250   three main concerns in high-resolution estimation of surface N_r concentration and

251   deposition based on satellite N_r observation. (1) How to effectively couple the satellite

252   high-resolution NO_2 and NH_3 column data with the vertical profiles simulated by an

253   ACTM, and then estimates the surface N_r concentrations? This step is the key to

254   simulate the dry N_r deposition. (2) How to construct a model for estimating dry N_r

255   deposition including all major N_r species based on satellite NO_2 and NH_3 column, and

256   then estimates the dry N_r deposition at a high spatial resolution? (3) How to combine

257   the high-resolution satellite NO_2 and NH_3 column data and ground-based monitoring

258   data to construct wet N_r deposition models, and then estimate the wet N_r deposition at

259   a high spatial resolution?

260   **3. Framework of Estimating Surface N_r Concentration and Deposition Using**

261   **Satellite Observation**

262   We give a framework of using satellite observation to estimate surface N_r

263   concentration and deposition as shown in **Fig. 1** based on recent advances.
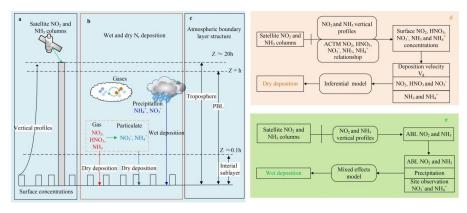

264

265   **Fig. 1 Schematic diagram of dry and wet N_r deposition.** (a) indicates satellite observed NO_2
266   and NH_3 column, and the vertical profiles by an ACTM; (b) shows dry and wet N_r deposition
267   including the major N_r species (gaseous NO_2, HNO_3, NH_3, particulate NO_3^- and NH_4^+, as well as
268   wet NO_3^- and NH_4^+ in precipitation); (c) illustrates atmospheric vertical structures including the
269   troposphere (satellite observation), atmospheric boundary layer (ABL), interfacial sub-layer; (d)
270   and (e) represent procedures of calculating the dry and wet N_r deposition.

271

272   **3.1.1 Conversion of Satellite NO_2 and NH_3 Column to Surface N_r Concentration**

273   An ACTM can simulate the vertical profiles of NO_2 and NH_3 with multiple layers

Atmospheric
Chemistry
and Physics
Discussions
Open Access
EGU

274   from the surface to the troposphere. For example, the GEOS-Chem ACTM includes

275   47 vertical layers from the earth surface to the top of the stratosphere. Most previous

276   studies estimated the ratio of surface N_r concentration (at the first layer) to total

277   columns by an ACTM, and then multiply the ratio by satellite columns to estimate

278   satellite-derived surface concentration (Geddes et al., 2016;Graaf et al., 2018;Nowlan

279   et al., 2014).

280   Another approach tries to fit general vertical profiles of NO_2 and NH_3 (Zhang et al.,

281   2017;Liu et al., 2017b;Liu et al., 2017c), and then estimate the ratio of N_r

282   concentration at any height to total N_r columns, and finally multiply the ratio by

283   satellite NO_2 and NH_3 columns. This approach has an advantage compared with the

284   previous one for that NO_2 and NH_3 concentration at all altitude included in ACTM

285   simulations can be estimated.

286   Taking the estimation of surface NO_2 concentration using the latter approach as an

287   example, the methods and steps are introduced in the following.

288   Step 1: Calculate the monthly mean NO_2 concentrations at all layers simulated by an

289   ACTM.

290   Step 2: Construct the vertical profile function of NO_2. Multiple Gaussian functions are

291   used to fit the vertical distribution of NO_2 based on the monthly NO_2 concentrations at

292   all layers calculated in Step 1, in which the independent variable is the height

293   (altitude), and the dependent variable is NO_2 concentration at a certain height.

294   The basic form of single Gaussian function is (Zhang et al., 2017;Liu et al., 2017b;Liu

295   et al., 2017c;Whitburn et al., 2016):

296    $\rho = \rho_{max} e^{-(\frac{Z-Z_0}{\sigma})^2}$ (1)

297   where Z is the height of a layer in the ACTM; ρ_{max}, Z_o and σ are the maximum NO_2

298   concentration, the corresponding height with the maximum NO_2 concentration and the

299   thickness of NO_2 concentration layer (one standard error of Gaussian function).

300   There are two basic forms of profile shapes of NO_2: (1) NO_2 concentration reaches the

301   maximum concentration when reaching a certain height ($Z_o \neq 0$). As the height

302   increases, the NO_2 concentration begins to decline; (2) NO_2 concentration is basically

303   concentrated on the earth surface ($Z_o = 0$). These two cases are the ideal state of the

304   vertical distribution of NO_2 concentration. In reality, single Gaussian fitting may not

305   capture the vertical distribution of NO_2 well. To improve the accuracy of fitting, the

306   sum of multiple Gaussian functions can be used:

307    $\rho(Z) = \sum_{i=1}^{n} \rho_{max,i} e^{-(\frac{Z - Z_{0,i}}{\sigma_i})^2}$ (2)

308   Step 3: Calculate the ratio of NO_2 concentration at the height of h_G to total columns

309   ($\int_0^{h_{trop}} \rho(Z)\,dx$), and then multiply the ratio by satellite column (S_{trop}). The

310   satellite-derived N_r concentration at the height of h_G can be calculated as:

311    $S_{G\_NO2} = S_{trop} \times \frac{\rho(h_G)}{\int_0^{h_{trop}} \rho(Z)dx}$ (3)

312   Step 4: Convert the instantaneous satellite-derived surface NO_2 concentration (S_{G_NO2})

313   to daily average ($S_{G\_NO2}*$) using the ratio of average surface NO_2 concentration

314   (G_{ACTM}^{1-24}) to that at satellite overpass time ($G_{ACTM}^{overpass}$) by an ACTM:

315    $S_{G\_NO2}* = \frac{G_{ACTM}^{1-24}}{G_{ACTM}^{overpass}} \times S_{G\_NO2}$ (4)

316   The method for estimating the surface NH_3 concentration ($S_{G\_NH3}*$) is similar to that

317   for estimating the surface NO_2 concentration.

318   **3.1.2 Estimating Surface Concentration of Other N_r Species**

319   At present, only NO_2 and NH_3 column can be retrieved reliably, and there are no

320   reliable satellite retrievals of HNO_3, NH_4^+ and NO_3^-. For example, the IASI HNO_3

321   product is still in the stage of data development and verification (Ronsmans et al.,

322 2016). Previous studies firstly derive the relationship between N_r species by an

323 ACTM or by ground-based measurements, and then use the relationship to convert

324 satellite-derived surface NO_2 and NH_3 concentration (S_{G_NH3} *) to HNO_3, NH_4^+ and

325 NO_3^- concentrations:

326
$$\begin{cases} G_{S\_NO3} = S_{G\_NO2} *\times \frac{G_{ACTM\_NO3}}{G_{ACTM\_NO2}} \\ G_{S\_HNO3} = S_{G\_NO2} *\times \frac{G_{ACTM\_HNO3}}{G_{ACTM\_NO2}} \quad (5) \\ G_{S\_NH4} = S_{G\_NH3} *\times \frac{G_{ACTM\_NH4}}{G_{ACTM\_NH3}} \end{cases}$$

327 $\frac{G_{ACTM\_NO3}}{G_{ACTM\_NO2}}$, $\frac{G_{ACTM\_HNO3}}{G_{ACTM\_NO2}}$, $\frac{G_{ACTM\_NH4}}{G_{ACTM\_NH3}}$ is the estimated ratio of between NO_2 and NO_3^-,

328 NO_2 and HNO_3, NH_3 and NH_4^+.

3.1.3 Dry Deposition of N_r

330 The resistance of dry N_r deposition mainly comes from three aspects: aerodynamic

331 resistance (R_a), quasi laminar sub-layer resistance (R_b) and canopy resistance (R_c).

332 The V_d can be expressed as

333 $V_d = \frac{1}{R_a+R_b+R_c} + v_g$ (6)

334 V_g is gravitational settling velocity. For gases, the V_g is negligible ($V_g=0$).

335 Dry NO_2, NO_3^-, HNO_3, and NH_4^+ deposition can be calculated by:

336 $F = G_S \times V_d$ (7)

337 Unlike above species, NH_3 is bi-directional, presenting both upward and downward

338 fluxes. There is a so-called "canopy compensation point" (C_o) controlling dry NH_3

339 deposition. Dry NH_3 deposition can be calculated by:

340 $F = (G_{S\_NH3} - C_o) \times V_d$ (8)

341 The calculation of C_o is very complex including the leaf stomatal and soil emission

342 potentials related to the meteorological factors, the plant growth stage and the canopy

343 type. The satellite-based methods usually neglected this complex process and set C_o

Atmospheric
Chemistry
and Physics
Discussions

Open Access

EGU

344   as zero (Graaf et al., 2018;Kharol et al., 2018) or set fixed values in each land use

345   type based on ground-based measurements (Jia et al., 2016).

346   **3.1.4 Wet Deposition of N_r**

347   The satellite-based estimation of wet N_r deposition can be simplified as the product of

348   the concentration of N_r (C), precipitation (P) and scavenging coefficient (w) (Pan et

349   al., 2012). Satellite NO_2 and NH_3 can be used to indicate the oxidized N_r and reduced

350   N_r; precipitation (P) can be obtained from ground monitoring data or reanalysis data

351   (such as NCEP). However, the scavenging coefficient (w) is usually highly uncertain.

352   To improve the accuracy of estimation, a mixed-effects model (Liu et al.,

353   2017a;Zhang et al., 2018) is proposed to build the relationship between satellite NO_2

354   and NH_3, precipitation and ground monitoring wet N_r deposition:

355     $\text{WetN}_{ij} = \alpha_j + \beta_i \times P_{ij} \times (S_{ABL})_{ij} + \varepsilon_{ij}$ (9)

356     $S_{ABL} = S_{trop} \times \dfrac{\int_0^{ABL} \rho(Z)dx}{\int_0^{h_{trop}} \rho(Z)dx}$ (10)

357   WetN_{ij} is wet NO_3^--N or NH_4^+-N deposition at month i and site j; $(S_{ABL})_{ij}$ is the

358   atmospheric boundary layer (ABL) NO_2 or NH_3 columns at month i and site j; P_{ij} is

359   precipitation at month i and site j; β_i and α_j are the slope and intercept of random

360   effects, representing seasonal variability and spatial effects；ε_{ij} represents the random

361   error at month i and site j.

362   The scavenging process of wet N_r deposition usually starts from the height of rainfall

363   rather than the top of the troposphere, so it is more reasonable to use NO_2 and NH_3

364   column below the height of rainfall to build the wet N_r deposition model. The NO_2

365   and NH_3 column within ABL is used to build the wet deposition model since

366   precipitation height is close to the height of the ABL (generally less than 2-3 km).

4. Satellite-derived Surface N_r Concentration and Deposition

4.1 Surface NO_2 Concentration and Oxidized N_r Deposition

The spatial resolutions of global ACTMs and therefore modeled surface N_r concentration are very coarse (for example, the spatial resolution of the global version of GEOS-Chem is $2^{o} \times 2.5^{o}$). Thus it can be hard to estimate surface N_r concentration and deposition at a fine resolution at a global scale by ACTMs alone. Instead, the satellite N_r retrievals have a high spatial resolution and can reveal more spatial details than ACTM simulations.

Cheng et al. (Cheng et al., 2013) and Jia et al. (Jia et al., 2016) established a linear model between the surface NO_2 concentration and NO_2 column by assuming the ratio of the surface NO_2 concentration to the tropospheric NO_2 column to be fixed, and then used the linear model to convert satellite NO_2 columns to surface NO_2 concentration, and finally estimated dry NO_2 deposition using the inferential method. However, these statistical methods by Cheng et al. (Cheng et al., 2013) and Jia et al. (Jia et al., 2016) are highly dependent on the ground-based measurements, and the established linear models may be not effective over regions with few monitoring sites. A comprehensive study (Nowlan et al., 2014) estimated global surface NO_2 concentration during 2005-2007 by multiplying OMI tropospheric NO_2 columns by the ACTM-modeled ratio between surface NO_2 concentration and tropospheric column (**Fig. 2**). Nowlan et al. (Nowlan et al., 2014) also estimated dry NO_2 deposition using the OMI-derived surface NO_2 concentration combining the modeled V_d during 2005-2007. This approach followed an earlier study (Lamsal et al., 2008), that focus on North America. As reported by Lamsal et al. (Lamsal et al., 2008), the satellite-derived surface NO_2 concentration was generally lower than ground-based NO_2 observations, ranging from -17% to -36% in North America. Kharol et al.

392   (Kharol et al., 2015) used a similar method and found the satellite-derived surface

393   NO$_2$ concentration was only half of the ground-measured values in North America

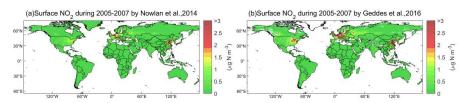394   (Kharol et al., 2015).

396   **Fig. 2** Satellite-derived surface NO$_2$ concentration during 2005-2007 by Nowlan et al. (Nowlan et
397   al., 2014) (a) and by Geddes et al. (Geddes et al., 2016) (b). We gained the surface NO$_2$
398   concentration by Nowlan et al. (Nowlan et al., 2014) and by Geddes et al. (Geddes et al., 2016) at
399   the web: http://fizz.phys.dal.ca/~atmos/martin/?page_id=232.

401   Geddes et al. (Geddes et al., 2016) followed previous studies, and used NO$_2$ column

402   from the GOME, SCIAMACHY, and GOME-2 to estimate surface NO$_2$ concentration.

403   Although Geddes et al. (Geddes et al., 2016) did not evaluate their results with

404   ground-based observation, it is obvious that their surface NO$_2$ estimates were higher

405   than Nowlan's estimates (Nowlan et al., 2014) based on OMI (**Fig. 2**). This may be

406   because the OMI-derived NO$_2$ column is much lower than that derived by GOME,

407   SCIAMACHY, and GOME-2, especially over polluted regions. For example, in China,

408   the OMI NO$_2$ column is about 30% lower than that of SCIAMACHY and GOME-2

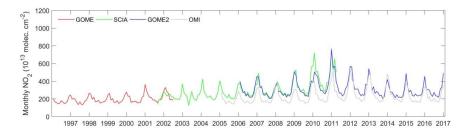409   consistently (**Fig. 3**).

411   **Fig. 3** An example of the time series of monthly NO$_2$ column retrieved by GOME, SCIAMACHY,
412   GOME2 and OMI in China. We obtained the GOME, SCIAMACHY, GOME2 and OMI data from
413   http://www.temis.nl/airpollution/no2.html.

415   Larkin et al. (Larkin et al., 2017) established a land-use regression model to estimate

416   global surface NO_2 concentration by combining satellite-derived surface NO_2

417   concentration by Geddes et al. (Geddes et al., 2016) and ground-based annual NO_2

418   measurements. The study by Larkin et al. (Larkin et al., 2017) can be considered as

419   using the ground-based annual measurements to adjust the satellite-derived surface

420   NO_2 concentration by Geddes et al. (Geddes et al., 2016), which helped reduce the

421   discrepancy between satellite-derived and ground-measured NO_2 concentration. The

422   regression model captured 54% of global NO_2 variation, with an absolute error of 2.32

423    $\mu g\ N\ m^{-3}$.

424   Zhang et al. (Zhang et al., 2017) followed the framework in **Sect. 3** to estimate the

425   OMI-derived surface NO_2 concentration (at ~50 m) in China, and found good

426   agreement with ground-based surface NO_2 concentration from the NNDMN at yearly

427   scale (slope=1.00, R^2=0.89). The methods by Zhang et al. (Zhang et al., 2017) can

428   also generate OMI-derived NO_2 concentration at any height by the constructed NO_2

429   vertical profile. Zhang et al. (Zhang et al., 2017) also estimated dry NO_2 deposition

430   using the OMI-derived surface NO_2 concentration combining the modeled V_d during

431   2005-2016. Based on Zhang's estimates, the Gaussian function can well simulate the

432   vertical distribution of NO_2 from an ACTM (MOZART) (Emmons et al., 2010) with

433   99.64% of the grids having R^2 values higher than 0.99. This suggests that the

434   ACTM-simulated vertical distribution of NO_2 has a general pattern, which can be

435   emulated by Gaussian functions. Once a vertical profile was constructed, it can be

436   easily used to estimate NO_2 concentration at any height.

437   In this study, we used the framework in **Sect. 3** to estimate the OMI-derived surface

438   NO_2 concentration globally. To validate the OMI-derived surface NO_2 concentrations,

439   ground-measured surface NO_2 concentration in China, the US and Europe in 2014

440   was collected (**Fig. 4**). The total number of NO_2 observations in China, the US and

441 Europe are 43, 373 and 88 respectively. The OMI-derived annual average for all sites

442 was 3.74 µg N m^{-3}, which was close to the measured average (3.06 µg N m^{-3}). The R^2

443 between OMI-derived surface NO$_2$ concentrations and ground-based NO$_2$

444 measurements was 0.75 and the RMSE was 1.23 µg N m^{-3} (**Fig. 5**), which is better

445 than the modeling results by the GEOS-Chem ACTM (R^2=0.43, RMSE=1.93 µg N

446 m^{-3}). Satellite-based methods have the advantages of spatiotemporally continuous

447 monitoring N$_r$ at a higher resolution, which helps alleviate the problem of the coarse

448 resolution of ACTMs in estimating N$_r$ concentration and deposition.

449

450 **Fig. 4** Spatial distribution of measured surface NO$_2$ and NH$_3$ concentrations in 2014. For NO$_2$ (a),
451 the measured data in China, the US and Europe were obtained from the NNDMN, US-EPA and
452 EMEP, respectively; for NH$_3$ (b), the measured data in China, the US and Europe were obtained
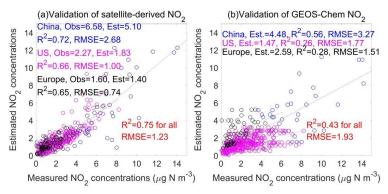453 from the NNDMN, US-AMoN and EMEP, respectively

454

455

456 **Fig. 5** Comparison between annual mean satellite-derived and ground-measured surface NO$_2$
457 concentrations (a), and comparison between annual mean modeled (by an ACTM as GEOS-Chem)
458 and ground-measured surface NO$_2$ concentrations (b). The ground-based monitoring sites are
459 shown in **Fig. 4**.

460

461 For NO$_3^-$ and HNO$_3$, previous studies firstly constructed the relationship between NO$_2$,

462 NO$_3^-$ and HNO$_3$, and found a relatively high linear relationship between NO$_2$, NO$_3^-$,

463   and HNO_3 at a monthly or yearly scale. For example, Jia et al. (Jia et al., 2016) found

464   a linear relationship between NO_2 and NO_3^-, HNO_3 concentration at annual scale

465   (R^2=0.70). Similarly, based on the ground-based measurements in the NNDMN, a

466   high correlation was found between surface NO_2 and NO_3^- concentration at monthly

467   or annual timescales (**Fig. 6**) (Liu et al., 2017c). Using these linear relationships and

468   satellite-derived surface NO_2 concentration, the annual mean surface NO_3^- and HNO_3

469   can be estimated. Alternatively, the relationship of NO_2, NO_3^- and HNO_3 can also be

470   modeled by an ACTM. For example, a strong relationship of tropospheric NO_2, NO_3^-

471   and HNO_3 column was simulated over all months by an ACTM, with the correlation

472   ranging from 0.69 to 0.91 (Liu et al., 2017a). But, over shorter timescales, the

473   relationship between NO_2, NO_3^- and HNO_3 may be nonlinear, which we should be

474   cautious about when estimating surface NO_3^- and HNO_3 concentration from NO_2
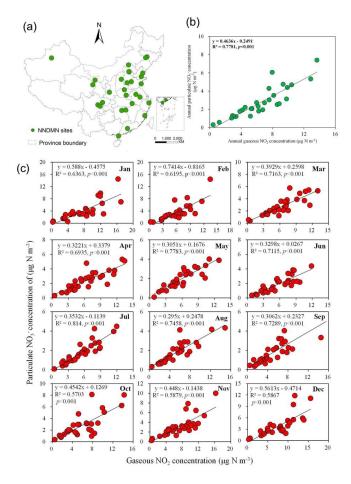
475   concentration.

Fig. 6 Correlation between surface NO_2 and particulate NO_3^- concentration in the NNDMN at annual and monthly scales, which were adopted from Liu et al. (Liu et al., 2017c). (a) indicates the spatial locations of monitoring sites in the NNDMN; (b) and (c) represent yearly and monthly relationship between surface NO_2 and particulate NO_3^- concentration, respectively.

For the wet N_r deposition, Liu et al. (Liu et al., 2017a) followed the framework in

Sect. 3 to estimate wet nitrate deposition using ABL NO_2 columns derived from OMI

NO_2 column and NO_2 vertical profile from an ACTM (MOZART), and precipitation

by a mixed-effects model showing the proposed model can achieve high predictive

power for monthly wet nitrate deposition over China (R=0.83, RMSE=0.72).

4.2 Surface NH_3 Concentration and Reduced N_r Deposition

With the development of atmospheric remote sensing of NH_3, some scholars have

489   estimated surface NH_3 concentration and dry NH_3 deposition based on the satellite

490   NH_3 column data. Assuming the ratio between the surface NH_3 concentration to the

491   NH_3 column was fixed, Yu et al. (Yu et al., 2019) applied a linear model to convert

492   satellite NH_3 columns to surface NH_3 concentration and estimated dry NH_3 deposition

493   in China using the inferential method. But Yu et al. (Yu et al., 2019) did not consider

494   the spatial variability of the vertical profiles of NH_3, which may cause a large

495   uncertainty in estimating surface NH_3 concentration.

496   In Western Europe, Graaf et al. (Graaf et al., 2018) used the ratio of the surface NH_3

497   concentration (in the bottom layer) to total NH_3 column from an ACTM to convert the

498   IASI NH_3 column to surface NH_3 concentration, and then estimated dry NH_3

499   deposition combining the modeled deposition velocity and IASI-derived surface NH_3

500   concentration. Similarly, in North America, Kharol et al. (Kharol et al., 2018)

501   estimated the dry NH_3 deposition by the CrIS-derived surface NH_3 concentration and

502   deposition velocity of NH_3. They found a relatively high correlation (R=0.76)

503   between the CrIS-derived surface NH_3 concentration and AMoN measurements during

504   warm seasons (from April to September) in 2013 (**Fig. 7**). Over China, Liu et al. (Liu

505   et al., 2017b) found a higher correlation (R=0.81) between IASI-derived surface NH_3

506   concentrations and the measured surface NH_3 concentrations than those from an
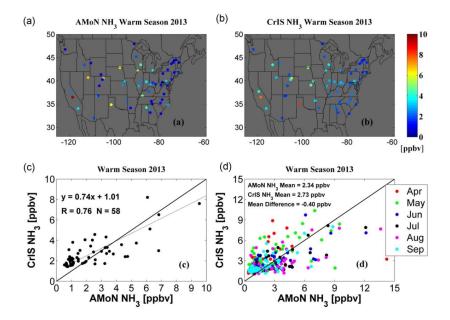
507   ACTM (R=0.57, **Fig. 8**).

Fig. 7 Comparisons of the measured surface NH_3 concentration by the AMoN and CrIS-derived surface NH_3 concentration in the US during warm season (April-September) in 2013 (Kharol et al., 2018). (a) and (b) indicate measured and CrIS-derived surface NH_3 concentration at the AMoN sites, respectively; (c) represents the comparison of averaged surface NH_3 concentration during warm months between CrIS-derived estimates and measurements, while (d) indicates the comparison of monthly surface NH_3 concentration between CrIS-derived estimates and measurements.
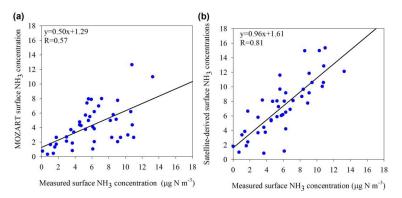

Fig. 8 Comparisons of the measured surface NH_3 concentration with IASI-derived surface NH_3 concentration at the NNDMN sites over China (Liu et al., 2017b). (a) indicates the comparison of measured and modeled surface NH_3 concentration from an ACTM (MOZART), and (b) represents the comparison of the measured and IASI-derived surface NH_3 concentration.

Liu et al. (Liu et al., 2019) followed the framework in **Sect. 3** to estimate the

IASI-derived surface NH_3 concentration (at the middle height of the first layer by an

Atmospheric
Chemistry
and Physics
Discussions

525 ACTM) (**Fig. 9**), and found a good agreement with ground-based surface NH_3

526 concentration. The correlation between the measured and satellite-derived annual

527 mean surface NH_3 concentrations over all sites was 0.87 as shown in **Fig. 10**, while

528 the average satellite-derived and ground-measured surface NH_3 concentration was

529 2.52 and 2.51 μg N m^{-3} in 2014 at the monitoring sites, respectively. The

530 satellite-derived estimates achieved a better accuracy (R^2=0.76, RMSE = 1.50 μg N

531 m^{-3}) than an ACTM (GEOS-Chem, R^2=0.54, RMSE = 2.14 μg N m^{-3}).
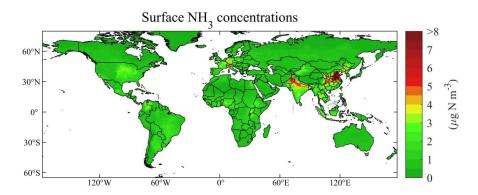

Surface NH_3 concentrations

532

533 **Fig. 9** Spatially satellite-based surface NH_3 estimates in 2014 (Liu et al., 2019). The global surface
534 NH_3 concentration datasets have been released on the website:
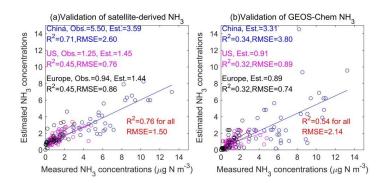535 https://zenodo.org/record/3546517#.Xj6I4GgzY2w.
536

537

538 **Fig. 10** Comparison between yearly satellite-based and measured surface NH_3 concentrations (a),
539 and comparison between yearly modeling (by an ACTM as GEOS-Chem) and measured surface
540 NH_3 concentrations (b) (Liu et al., 2019). The ground-based monitoring sites are shown in **Fig. 4**.
541

542 The proposed methods (Liu et al., 2019) can also estimate NH_3 concentration at any

543   height using the constructed vertical profile function of NH_3. The Gaussian function

544   can well emulate the vertical distribution of NH_3 from an ACTM outputs with 99% of

545   the grids having R^2 values higher than 0.90 (**Fig. 11**). This means, for regional and

546   global estimation, the vertical distribution of NH_3 concentration has a general pattern,

547   which can be mostly emulated by the Gaussian function. Once a global NH_3 vertical

548   profile was simulated, it can be easily used to estimate satellite-derived NH_3

549   concentration at any height. We can also estimate dry NH_3 deposition using the

550   IASI-derived surface NH_3 concentration combining the modeled V_d. To date, there are

551   still no studies developing satellite-based methods to estimate the wet reduced N_r
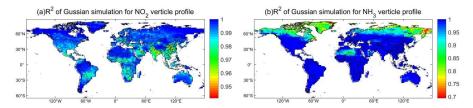
552   deposition on a regional scale.

553

Fig. 11 Spatial distributions of R^2 for Gaussian function by simulating NH_3 and NO_2 vertical
profiles. This is an example of Gaussian fitting using 47 layers' NH_3 and NO_2 concentration from
an ACTM (GEOS-Chem).

558   **5. Trends of Surface N_r Concentration and Deposition by Satellite-based**

559   **Methods**

560   The N_r concentration and deposition modeled by ACTMs are highly dependent on the

561   accuracy of input N_r emissions. The methods commonly used to estimate

562   anthropogenic N_r emissions are based on the data of human activities and emission

563   factors, which can be highly uncertain. The ACTM methods driven by N_r emission

564   inventory have relatively poor timeliness, and have limitations in monitoring the

565   recent trends of N_r deposition.

566   Satellite-based methods provide a simple, fast and relatively objective way to

567   monitoring N_r deposition at a high resolution, and less susceptible to the errors in the

568   assumptions that emission inventories are compiled based on, particularly the lack of

569   reliable data over developing countries (Crippa et al., 2018). With such advantages,

570   researchers developed the satellite-based methods to estimate surface N_r concentration,

571   deposition and even emissions. Satellite-based methods have advantages in

572   monitoring the recent trends of N_r deposition. Geddes et al. (Geddes and Martin, 2017)

573   used NO_2 column from the GOME, SCIAMACHY, and GOME-2 to estimate

574   satellite-derived NO_x emissions, and then used the calibrated NO_x emission inventory

575   to drive an ACTM to simulate the long-term oxidized N_r deposition globally. They

576   found oxidized N_r deposition from 1996 to 2014 decreased by 60% in Eastern US,

577   doubled in East China, and declined by 20% in Western Europe (**Fig. 12**). We use the

578   datasets by Geddes et al. (Geddes and Martin, 2017) to calculate the trends of total

579   oxidized N_r deposition during 1996-2014. It is obvious that two completely opposite

580   trends exist: (1) in East China with a steep increase of higher than 0.5 kg N ha^{-1} y^{-1}

581   and (2) East US with a steep decrease of lower than -0.5 kg N ha^{-1} y^{-1}. Although it is

582   not a direct way to use satellite N_r observation to estimate N_r deposition, the method

583   of estimating trends of N_r deposition by Geddes et al. (Geddes and Martin, 2017) can

584   be considered effective since it took account of the changes of both NO_x emission and

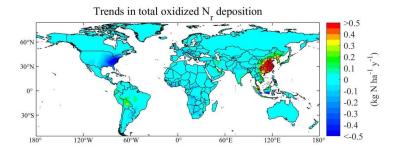585   climate by an ACTM.

586

587   **Fig. 12** Gridded annual changes of total oxidized N_r deposition simulated by GEOS-Chem
588   constrained with GOME, SCIAMACHY, and GOME-2 NO_2 retrievals during 1996-2014 (Geddes
589   and Martin, 2017). We gained the generated datasets
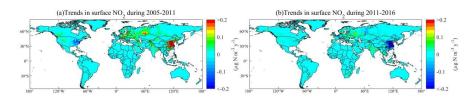
590   (http://fizz.phys.dal.ca/~atmos/martin/?page_id=1520) by Geddes et al. (Geddes and Martin,
591   2017), and calculated the trends using the linear methods.
592

593   Some researchers developed a more direct way to infer the trends of surface N_r

594   concentration and deposition. Geddes et al. (Geddes et al., 2016) presented a

595   comprehensive long-term global surface NO_2 concentration estimate (at 0.1°

596   resolution using an oversampling approach) between 1996 and 2012 by using NO_2

597   column from the GOME, SCIAMACHY, and GOME-2. The surface NO_2

598   concentration in North America (the US and Canada) decreased steeply, followed by

599   Western Europe, Japan and South Korea, while approximately tripled in China and

600   North Korea (Geddes et al., 2016). Jia et al. (Jia et al., 2016) established a simple

601   linear regression model based on OMI NO_2 column and ground-based surface N_r

602   concentration, and then estimated the trends of dry N_r deposition globally between

603   2005 and 2014. They found that dry N_r deposition in Eastern China increased rapidly,

604   while in the Eastern US, Western Europe, and Japan dry N_r deposition has decreased

605   in recent decades.

606   We split the time span of 2005-2016 into two periods: 2005-2011 and 2011-2016, as

607   surface NO_2 concentration shows opposite trend in China in these two periods. The

608   magnitudes of both growth and decline in surface NO_2 concentration in China are

609   most pronounced worldwide in the two periods (**Fig. 13**). During 2005-2011, apart

610   from Eastern China with the largest increase in surface NO_2 concentration, there are

611   also several areas with increasing trends such as Northwest and East India (New Delhi

612   and Orissa), Western Russia, Eastern Europe (Northern Italy), Western US (Colorado

613   and Utah), Northwestern US (Seattle and Portland), Southwestern Canada (Vancouver,

614   Edmonton, Calgary), Northeast Pakistan and Northwest Xinjiang (Urumqi). Notably,

615   the biggest decreases in surface NO_2 concentration during 2005-2011 occurred in

616   Eastern US and Western EU (North France, South England, and West German).

27

617   During 2011-2016, due to the strict control of NO_x emissions, Eastern China had the

618   largest decrease in surface NO_2 concentration than elsewhere worldwide, followed by

619   Western Xinjiang, Western Europe and some areas in Western Russia.

620

621   **Fig. 13** Gridded annual changes in surface NO_2 concentrations gained by OMI retrievals during
622   2005-2011 (a) and during 2011-2016 (b) in this study. We have released the global surface NO_2
623   concentrations during 2005-2016 available at the website:
624   https://zenodo.org/record/3546517#.Xj6I4GgzY2w.
625

626   Liu et al. (Liu et al., 2019) estimated surface NH_3 concentration globally during

627   2008-2016 using satellite NH_3 retrievals by IASI. A large increase of surface NH_3

628   concentrations was found in Eastern China, followed by Northern Xinjiang province

629   in China during 2008-2016 (**Fig. 14**). Satellite-based methods have been proven as an

630   effective and unique way to monitoring the trends of global N_r concentration and

631   deposition. To date, there are still few studies reporting the satellite-derived trends of

632   reduced N_r deposition on a global scale.
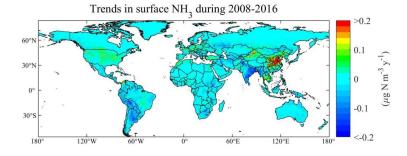

633

634   **Fig. 14** Gridded annual changes in surface NH_3 concentrations gained by IASI retrievals during
635   2008-2016 (Liu et al., 2019). We have released the global surface NH_3 concentrations during
636   2008-2016 at the website: https://zenodo.org/record/3546517#.Xj6I4GgzY2w.
637

638   **6. Remaining Challenges for Estimating N_r Deposition Using Satellite**

639   **Observation**

640   First, the reduced N_r deposition plays an important contribution to total N_r deposition.

641   NH_3 exhibits bi-directional air-surface exchanges. The NH_3 compensation point

642   (Farquhar et al., 1980) is also an important and highly variable factor controlling dry

643   NH_3 deposition (Schrader et al., 2016;Zhang et al., 2010). However, the current

644   existing satellite-based methods did not consider this bi-directional air-surface

645   exchange. It is important to better parameterize the NH_3 compensation point, and

646   assess the effects of bi-directional air-surface exchanges on estimating the dry NH_3

647   deposition.

648   Second, the existing satellite-based methods to estimate N_r deposition used the ratio

649   of the surface N_r concentration to the N_r column by an ACTM to convert satellite N_r

650   column to surface N_r concentration. However, the calculated ratio (by an ACTM) and

651   the satellite N_r column have different spatial resolutions, and previous studies usually

652   applied the modeled ratio directly or interpolate the ratio into the resolution of

653   satellite N_r column. This method assumes the relationship at coarse resolution by an

654   ACTM can also be effective in fine resolution as satellite indicated. When regional

655   studies are conducted, regional ACTMs coupled with another meteorological model

656   (e.g. WRF-Chem, WRF-CMAQ) (Grell et al., 2005;Wong et al., 2012) can be

657   configured to match the spatial resolution of satellite observation, but this is not as

658   viable for global ACTMs (e.g. MOZART, GEOS-Chem) due to differences in model

659   structures and computational cost. The modeled ratio of surface N_r concentration to

660   the N_r column may have variability at spatial scales finer than the horizontal

661   resolution of global ACTMs. The impact of such scale effect (at different spatial

662   scales) on estimated surface N_r concentration should be further studied.

663 Third, the satellite observation can only obtain reliable NO_2 and NH_3 column

664 presently, and there are no available high-resolution and reliable direct HNO_3, NO_3^-,

665 NH_4^+ retrievals. For HNO_3, NO_3^-, NH_4^+ concentrations, the satellite-based methods

666 often applied the satellite-derived NO_2 and NH_3 concentration and the relationship

667 between N_r species from an ACTM (or ground-based measurements) to estimate

668 surface HNO_3, NO_3^-, NH_4^+ concentration. With the development of satellite

669 technology, more and more N_r species can be detected, such as HNO_3. However, at

670 present, satellite HNO_3 products are not mature, and the spatial resolution is low.

671 Direct, high-resolution and reliable satellite monitoring of more N_r species is critical

672 to further developing the use of using atmospheric remote sensing to estimate N_r

673 deposition at global and regional scales.

674 Fourth, estimating wet N_r deposition using satellite NO_2 and NH_3 column remains

675 relatively uncommon. Further studies should focus on how to combine the

676 high-resolution satellite NO_2 and NH_3 column and the ground-based monitoring data

677 to build wet N_r deposition models to estimate wet N_r deposition at higher

678 spatiotemporal resolution. The proposed scheme to estimate the wet N_r deposition in

679 **Sect. 3** is statistical. On the other hand, the wet N_r deposition includes the scavenging

680 processes of in-cloud, under-cloud and precipitation. Processed-level knowledge and

681 models can benefit the estimation of wet N_r deposition using satellite NO_2 and NH_3

682 column.

683 **7. Conclusion**

684 The recent advances of satellite-based methods for estimating surface N_r

685 concentration and deposition have been reviewed. Previous studies have focused on

686 using satellite NO_2 column to estimate surface NO_2 concentrations and dry NO_2

687 deposition both regionally and globally. The research on calculating surface NH_3

Atmospheric
Chemistry
and Physics
Discussions

688   concentration and reduced N_r deposition by satellite NH_3 data is just beginning, and

689   some scholars have carried out estimating surface NH_3 concentration and dry NH_3

690   deposition on different spatial and temporal scales, but the research degree is still

691   relatively low. We present a framework of using satellite NO_2 and NH_3 column to

692   estimate N_r deposition based on recent advances. The proposed framework of using

693   Gaussian function to model vertical NO_2 and NH_3 profiles can be used to convert the

694   satellite NO_2 and NH_3 column to surface NO_2 and NH_3 concentration at any height

695   simply and quickly. The proposed framework of using satellite NO_2 and NH_3 column

696   to estimate wet N_r deposition is a statistical way, and further studies should be done

697   from a mechanism perspective. Finally, we summarized current challenges of using

698   satellite NO_2 and NH_3 column to estimate surface N_r concentration and deposition

699   including a lack of considering NH_3 bidirectional air-surface exchanges and the

700   problem of different spatial scales between an ACTM and satellite observation.

706   **Author contributions**. LL designed this study. LL, YYY and WX conducted the data

707   analysis. All co-authors contributed to the revision of the paper.

708   **Data availability**. OMI NO_2 datasets are available at

709   http://www.temis.nl/airpollution/no2.html. IASI NH_3 datasets are available at

710   https://cds-espri.ipsl.upmc.fr/etherTypo/index.php?id=1700&L=1. Surface NO_2

711   concentration during 2005-2007 obtained by Nowlan et al. (Nowlan et al., 2014) and

712   longterm estimates (1996-2012) by Geddes et al. (Geddes et al., 2016) are available at

713   http://fizz.phys.dal.ca/~atmos/martin/?page_id=232. Total oxidized N_r deposition

714   simulated by GEOS-Chem constrained with GOME, SCIAMACHY, and GOME-2

715   NO_2 retrievals during 1996-2014 (Geddes and Martin, 2017) is available at

716   http://fizz.phys.dal.ca/~atmos/martin/?page_id=1520. A database of atmospheric N_r

717   concentration and deposition from the nationwide monitoring network in China is

718   available at https://www.nature.com/articles/s41597-019-0061-2. Measured N_r

719   concentration and deposition datasets in the United States are available on the website:

720   https://www.epa.gov/outdoor-air-quality-data. Measured surface NO_2 and NH_3

721   concentration datasets in Europe are available at

722   https://www.nilu.no/projects/ccc/emepdata.html. Global surface NO_2 and NH_3

723   concentration data used to calculate the longterm trends in **Fig. 13** and **Fig. 14** have

724   been released on the website: https://zenodo.org/record/3546517#.Xj6I4GgzY2w.

725   **Competing interests**. The authors declare no competing financial interests.

726   **Reference**

727   Amos, H. M., Jacob, D. J., Holmes, C. D., Fisher, J. A., Wang, Q., Yantosca, R. M.,

728   Corbitt, E. S., Galarneau, E., Rutter, A. P., and Gustin, M. S.: Gas-particle partitioning

729   of atmospheric Hg(II) and its effect on global mercury deposition, Atmos. Chem.

730   Phys., 11, 29441-29477, 2012.

731   Beer, R., Shephard, M. W., Kulawik, S. S., Clough, S. A., Eldering, A., Bowman, K.

732   W., Sander, S. P., Fisher, B. M., Payne, V. H., Luo, M., Osterman, G. B., and Worden,

733   J. R.: First satellite observations of lower tropospheric ammonia and methanol,

734   Geophys. Res Lett., 35, 1-5, 10.1029/2008GL033642, 2008.

735   Bobbink, R., Hicks, K., Galloway, J., Spranger, T., Alkemade, R., Ashmore, M.,

736   Bustamante, M., Cinderby, S., Davidson, E., Dentener, F., Emmett, B., Erisman, J.-W.,

737 Fenn, M., Gilliam, F., Nordin, A., Pardo, L., and De Vries, W.: Global assessment of

738 nitrogen deposition effects on terrestrial plant diversity: a synthesis, Ecological

739 Applications, 20, 30-59, doi:10.1890/08-1140.1, 2010.

740 Boersma, K. F., Eskes, H. J., Dirksen, R. J., van der A, R. J., Veefkind, J. P., Stammes,

741 P., Huijnen, V., Kleipool, Q. L., Sneep, M., Claas, J., Leitão, J., Richter, A., Zhou, Y.,

742 and Brunner, D.: An improved tropospheric NO_2 column retrieval algorithm for the

743 Ozone Monitoring Instrument, Atmospheric Measurement Techniques, 4, 1905-1928,

744 10.5194/amt-4-1905-2011, 2011.

745 Canfield, D. E., Glazer, A. N., and Falkowski, P. G.: The evolution and future of

746 Earth's nitrogen cycle, Science, 330, 192-196, 2010.

747 Cao, G. L., Zhang, X. Y., and Gong, S. L.: Emission inventories of primary particles

748 and pollutant gases for China, Science Bulletin, 56, 781-788, 2011.

749 Cheng, M., Jiang, H., Guo, Z., Zhang, X., and Lu, X.: Estimating NO_2 dry deposition

750 using satellite data in eastern China, Int. J. Remote Sens., 34, 2548-2565, 2013.

751 Coheur, P.-F., Clarisse, L., Turquety, S., Hurtmans, D., and Clerbaux, C.: IASI

752 measurements of reactive trace species in biomass burning plumes, Atmos. Chem.

753 Phys., 9, 5655-5667, 2009.

754 Crippa, M., Guizzardi, D., Muntean, M., Schaaf, E., Dentener, F., van Aardenne, J. A.,

755 Monni, S., Doering, U., Olivier, J. G. J., Pagliari, V., and Janssens-Maenhout, G.:

756 Gridded emissions of air pollutants for the period 1970–2012 within EDGAR v4.3.2,

757 Earth Syst. Sci. Data, 10, 1987-2013, 10.5194/essd-10-1987-2018, 2018.

758 Dammers, E., Palm, M., Van Damme, M., Vigouroux, C., Smale, D., Conway, S.,

759   Toon, G. C., Jones, N., Nussbaumer, E., Warneke, T., Petri, C., Clarisse, L., Clerbaux,

760   C., Hermans, C., Lutsch, E., Strong, K., Hannigan, J. W., Nakajima, H., Morino, I.,

761   Herrera, B., Stremme, W., Grutter, M., Schaap, M., Wichink Kruit, R. J., Notholt, J.,

762   Coheur, P. F., and Erisman, J. W.: An evaluation of IASI-NH$_3$ with ground-based

763   Fourier transform infrared spectroscopy measurements, Atmos. Chem. Phys., 16,

764   10351-10368, 10.5194/acp-16-10351-2016, 2016.

765   David, F, M, C., U, S., MA, S., JN, C., S, R., LJ, S., A, J., B, G., and JN, G.: The

766   global nitrogen cycle in the twenty-first century, Philosophical Transactions of the

767   Royal Society of London, 368, 20130164, 2013.

768   Emmons, L., Walters, S., Hess, P., Lamarque, J.-F, Pfister, G., Fillmore, D., Granier,

769   C., Guenther, A., Kinnison, D., and Laepple, T.: Description and evaluation of the

770   Model for Ozone and Related chemical Tracers, version 4 (MOZART-4),

771   Geoscientific Model Development, 3, 43-67, 2010.

772   Erisman, J. W., Sutton, M. A., Galloway, J., Klimont, Z., and Winiwarter, W.: How a

773   century of ammonia synthesis changed the world, Nat. Geosci., 1, 636-639, 2008.

774   Farquhar, G. D., Firth, P. M., Wetselaar, R., and Weir, B.: On the Gaseous Exchange

775   of Ammonia between Leaves and the Environment: Determination of the Ammonia

776   Compensation Point, Plant Physiology, 66, 710-714, 10.1104/pp.66.4.710, 1980.

777   Galloway, J. N., Dentener, F. J., Capone, D. G., Boyer, E. W., Howarth, R. W.,

778   Seitzinger, S. P., Asner, G. P., Cleveland, C., Green, P., and Holland, E.: Nitrogen

779   cycles: past, present, and future, Biogeochemistry, 70, 153-226, 2004a.

780   Galloway, J. N., Dentener, F. J., Capone, D. G., Boyer, E. W., Howarth, R. W.,

781   Seitzinger, S. P., Asner, G. P., Cleveland, C. C., Green, P. A., Holland, E. A., Karl, D.

782   M., Michaels, A. F., Porter, J. H., Townsend, A. R., and Vöosmarty, C. J.: Nitrogen

783   Cycles: Past, Present, and Future, Biogeochemistry, 70, 153-226,

784   10.1007/s10533-004-0370-0, 2004b.

785   Galloway, J. N., Townsend, A. R., Erisman, J. W., Bekunda, M., Cai, Z., Freney, J. R.,

786   Martinelli, L. A., Seitzinger, S. P., and Sutton, M. A.: Transformation of the nitrogen

787   cycle: recent trends, questions, and potential solutions, Science, 320, 889-892, 2008.

788   Geddes, J. A., Martin, R. V., Boys, B. L., and van Donkelaar, A.: Long-term trends

789   worldwide in ambient NO_2 concentrations inferred from satellite observations,

790   Environmental Health Perspectives, 124, 281, 2016.

791   Geddes, J. A., and Martin, R. V.: Global deposition of total reactive nitrogen oxides

792   from 1996 to 2014 constrained with satellite observations of NO_2 columns, Atmos.

793   Chem. Phys., 1-44, 2017.

794   Graaf, S. C. v. d., Dammers, E., Schaap, M., and Erisman, J. W.: How are NH_3 dry

795   deposition estimates affected by combining the LOTOS-EUROS model with

796   IASI-NH3 satellite observations?, Atmos. Chem. Phys., 18, 13173-13196,

797   https://doi.org/10.5194/acp-2018-133, 2018.

798   Grell, G. A., Peckham, S. E., Schmitz, R., McKeen, S. A., Frost, G., Skamarock, W.

799   C., and Eder, B.: Fully coupled "online" chemistry within the WRF model, Atmos.

800   Environ., 39, 6957-6975, 2005.

801   Hoesly, R. M., Smith, S. J., Feng, L., Klimont, Z., Janssens-Maenhout, G., Pitkanen,

802   T., Seibert, J. J., Vu, L., Andres, R. J., Bolt, R. M., Bond, T. C., Dawidowski, L.,

Atmospheric
Chemistry
and Physics
Discussions

803   Kholod, N., Kurokawa, J. I., Li, M., Liu, L., Lu, Z., Moura, M. C. P., O'Rourke, P. R.,

804   and Zhang, Q.: Historical (1750–2014) anthropogenic emissions of reactive gases and

805   aerosols from the Community Emissions Data System (CEDS), Geosci. Model Dev.,

806   11, 369-408, 10.5194/gmd-11-369-2018, 2018.

807   Janssens, I. A., Dieleman, W., Luyssaert, S., Subke, J. A., Reichstein, M., Ceulemans,

808   R., Ciais, P., Dolman, A. J., Grace, J., Matteucci, G., Papale, D., Piao, S. L., Schulze,

809   E. D., Tang, J., and Law, B. E.: Reduction of forest soil respiration in response to

810   nitrogen deposition, Nat. Geosci., 3, 315, 10.1038/ngeo844

811   https://www.nature.com/articles/ngeo844#supplementary-information, 2010.

812   Jia, Y., Yu, G., Gao, Y., He, N., Wang, Q., Jiao, C., and Zuo, Y.: Global inorganic

813   nitrogen dry deposition inferred from ground-and space-based measurements,

814   Scientific reports, 6, 1-11, 2016.

815   Kharol, S. K., Martin, R. V., Philip, S., Boys, B., Lamsal, L. N., Jerrett, M., Brauer,

816   M., Crouse, D. L., Mclinden, C., and Burnett, R. T.: Assessment of the magnitude and

817   recent trends in satellite-derived ground-level nitrogen dioxide over North America,

818   Atmos. Environ., 118, 236-245, 2015.

819   Kharol, S. K., Shephard, M. W., McLinden, C. A., Zhang, L., Sioris, C. E., O'Brien, J.

820   M., Vet, R., Cady-Pereira, K. E., Hare, E., Siemons, J., and Krotkov, N. A.: Dry

821   Deposition of Reactive Nitrogen From Satellite Observations of Ammonia and

822   Nitrogen Dioxide Over North America, Geophys. Res Lett., 45, 1157-1166,

823   10.1002/2017GL075832, 2018.

824   Kim, T. W., Lee, K., Duce, R., and Liss, P.: Impact of atmospheric nitrogen deposition

Atmospheric
Chemistry
and Physics
Discussions

825   on phytoplankton productivity in the South China Sea, Geophys. Res Lett., 41, 3156–

826   3162, 2014.

827   Kuik, F., Lauer, A., Churkina, G., Denier van der Gon, H. A. C., Fenner, D., Mar, K.

828   A., and Butler, T. M.: Air quality modelling in the Berlin-Brandenburg region using

829   WRF-Chem v3.7.1: sensitivity to resolution of model grid and input data,

830   Geoscientific Model Development Discussions, 9, 4339-4363, 2016.

831   Lamarque, J. F., Kiehl, J., Brasseur, G., Butler, T., Cameron‑Smith, P., Collins, W.,

832   Collins, W., Granier, C., Hauglustaine, D., and Hess, P.: Assessing future nitrogen

833   deposition and carbon cycle feedback using a multimodel approach: Analysis of

834   nitrogen deposition, Journal of Geophysical Research: Atmospheres (1984–2012), 110,

835   2005.

836   Lamsal, L. N., Martin, R. V., van Donkelaar, A., Steinbacher, M., Celarier, E. A.,

837   Bucsela, E., Dunlea, E. J., and Pinto, J. P.: Ground-level nitrogen dioxide

838   concentrations inferred from the satellite-borne Ozone Monitoring Instrument, J.

839   Geophys. Res-Atmos., 113, 1-15, 10.1029/2007JD009235, 2008.

840   Lamsal, L. N., Martin, R. V., Parrish, D. D., and Krotkov, N. A.: Scaling relationship

841   for NO_2 pollution and urban population size: a satellite perspective, Environ. Sci.

842   Technol., 47, 7855-7861, 2013.

843   Larkin, A., Geddes, J. A., Martin, R. V., Xiao, Q., Liu, Y., Marshall, J. D., Brauer, M.,

844   and Hystad, P.: Global Land Use Regression Model for Nitrogen Dioxide Air

845   Pollution, Environ. Sci. Technol., 51, 6957-6964, 2017.

846   Larssen, T., Duan, L., and Mulder, J.: Deposition and leaching of sulfur, nitrogen and

847   calcium in four forested catchments in China: implications for acidification, Environ.

848   Sci. Technol., 45, 1192-1198, 2011.

849   Levine, S. Z., and Schwartz, S. E.: In-cloud and below-cloud scavenging of Nitric

850   acid   vapor,   Atmospheric   Environment   (1967),   16,   1725-1734,

851   https://doi.org/10.1016/0004-6981(82)90266-9, 1982.

852   Li, Y., Thompson, T. M., Damme, M. V., Chen, X., Benedict, K. B., Shao, Y., Day, D.,

853   Boris, A., Sullivan, A. P., and Ham, J.: Temporal and Spatial Variability of Ammonia

854   in Urban and Agricultural Regions of Northern Colorado, United States, Atmos. Chem.

855   Phys., 17, 1-50, 2017.

856   Liu, H., Jacob, D. J., Bey, I., and Yantosca, R. M.: Constraints from 210Pb and 7Be on

857   wet deposition and transport in a global three-dimensional chemical tracer model

858   driven by assimilated meteorological fields, J. Geophys. Res-Atmos., 106,

859   12109-12128, 10.1029/2000JD900839, 2001.

860   Liu, L., Zhang, X., Xu, W., Liu, X., Lu, X., Chen, D., Zhang, X., Wang, S., and Zhang,

861   W.: Estimation of monthly bulk nitrate deposition in China based on satellite NO_2

862   measurement by the Ozone Monitoring Instrument, Remote Sens. Environ., 199,

863   93-106, 2017a.

864   Liu, L., Zhang, X., Xu, W., Liu, X., Lu, X., Wang, S., Zhang, W., and Zhao, L.:

865   Ground Ammonia Concentrations over China Derived from Satellite and Atmospheric

866   Transport Modeling, Remote Sens., 9, 467, 2017b.

867   Liu, L., Zhang, X., Zhang, Y., Xu, W., Liu, X., Zhang, X., Feng, J., Chen, X., Zhang,

868   Y., Lu, X., Wang, S., Zhang, W., and Zhao, L.: Dry Particulate Nitrate Deposition in

869   China, Environ. Sci. Technol., 51, 5572-5581, 10.1021/acs.est.7b00898, 2017c.

870   Liu, L., Zhang, X., Wong, A. Y. H., Xu, W., Liu, X., Li, Y., Mi, H., Lu, X., Zhao, L.,

871   Wang, Z., and Wu, X.: Estimating global surface ammonia concentrations inferred

872   from   satellite   retrievals,   Atmos.   Chem.   Phys.,   19,   12051-12066,

873   10.5194/acp-2019-184, 2019.

874   Liu, X., Duan, L., Mo, J., Du, E., Shen, J., Lu, X., Zhang, Y., Zhou, X., He, C., and

875   Zhang, F.: Nitrogen deposition and its ecological impact in China: An overview,

876   Environ. Pollut., 159, 2251-2264, http://dx.doi.org/10.1016/j.envpol.2010.08.002,

877   2011.

878   Liu, X., Xu, W., Duan, L., Du, E., Pan, Y., Lu, X., Zhang, L., Wu, Z., Wang, X.,

879   Zhang, Y., Shen, J., Song, L., Feng, Z., Liu, X., Song, W., Tang, A., Zhang, Y., Zhang,

880   X., and Collett, J. L.: Atmospheric Nitrogen Emission, Deposition, and Air Quality

881   Impacts   in   China: an   Overview,   Curr.   Pollut.   Rep.,   3,   65-77,

882   10.1007/s40726-017-0053-9, 2017d.

883   Lu, X., Jiang, H., Zhang, X., Liu, J., Zhang, Z., Jin, J., Wang, Y., Xu, J., and Cheng,

884   M.: Estimated global nitrogen deposition using NO_2 column density, Int. J. Remote

885   Sens., 34, 8893-8906, 2013.

886   Mari, C., Jacob, D. J., and Bechtold, P.: Transport and scavenging of soluble gases in

887   a deep convective cloud, J. Geophys. Res-Atmos., 105, 22255-22268, 2000.

888   Nadelhoffer, K. J., Emmett, B. A., Gundersen, P., Kjønaas, O. J., Koopmans, C. J.,

889   Schleppi, P., Tietema, A., and Wright, R. F.: Nitrogen deposition makes a minor

890   contribution   to   carbon   sequestration   in   temperate   forests,   Nature,   398,   145,

891   10.1038/18205, 1999.

892   Nemitz, E., Flynn, M., Williams, P. I., Milford, C., Theobald, M. R., Blatter, A.,

893   Gallagher, M. W., and Sutton, M. A.: A Relaxed Eddy Accumulation System for the

894   Automated Measurement of Atmospheric Ammonia Fluxes, Water, Air and Soil

895   Pollution: Focus, 1, 189-202, 10.1023/A:1013103122226, 2001.

896   Nicolas, G., and Galloway, J. N.: An Earth-system perspective of the global nitrogen

897   cycle, Nature, 451, 293-296, 2008.

898   Nowlan, C., Martin, R., Philip, S., Lamsal, L., Krotkov, N., Marais, E., Wang, S., and

899   Zhang, Q.: Global dry deposition of nitrogen dioxide and sulfur dioxide inferred from

900   space-based measurements, Global Biogeochem. Cy., 28, 1025-1043, 2014.

901   Paerl, H. W., Gardner, W. S., Mccarthy, M. J., Peierls, B. L., and Wilhelm, S. W.:

902   Algal blooms: noteworthy nitrogen, Science, 346, 175, 2014.

903   Pan, Y., Wang, Y., Tang, G., and Wu, D.: Wet and dry deposition of atmospheric

904   nitrogen at ten sites in Northern China, Atmos. Chem. Phys., 12, 6515-6535, 2012.

905   Ronsmans, G., Langerock, B., Wespes, C., Hannigan, J. W., Hase, F., Kerzenmacher,

906   T., Mahieu, E., Schneider, M., Smale, D., Hurtmans, D., De Mazière, M., Clerbaux, C.,

907   and Coheur, P. F.: First characterization and validation of FORLI-HNO3 vertical

908   profiles   retrieved   from   IASI/Metop,   Atmos.   Meas.   Tech.,   9,   4783-4801,

909   10.5194/amt-9-4783-2016, 2016.

910   Schrader, F., Brümmer, C., Flechard, C. R., Wichink Kruit, R. J., van Zanten, M. C.,

911   Zöll, U., Hensen, A., and Erisman, J. W.: Non-stomatal exchange in ammonia dry

912   deposition models: comparison of two state-of-the-art approaches, Atmos. Chem.

Atmospheric
Chemistry
and Physics
Discussions

Open Access

EGU

913   Phys., 16, 13417-13430, 10.5194/acp-16-13417-2016, 2016.

914   Shen, J., Li, Y., Liu, X., Luo, X., Tang, H., Zhang, Y., and Wu, J.: Atmospheric dry

915   and wet nitrogen deposition on three contrasting land use types of an agricultural

916   catchment in subtropical central China, Atmos. Environ., 67, 415-424,

917   http://dx.doi.org/10.1016/j.atmosenv.2012.10.068, 2013.

918   Stevens, C. J., Dise, N. B., Mountford, J. O., and Gowing, D. J.: Impact of Nitrogen

919   Deposition on the Species Richness of Grasslands, Science, 303, 1876-1879,

920   10.1126/science.1094678, 2004.

921   Sutton, M. A., Tang, Y. S., Miners, B., and Fowler, D.: A New Diffusion Denuder

922   System for Long-Term, Regional Monitoring of Atmospheric Ammonia and

923   Ammonium, Water Air & Soil Pollution Focus, 1, 145-156, 2001.

924   Sutton, M. A., Bleeker, A., Howard, C. M., Bekunda, M., Grizzetti, B., Vries, W. D.,

925   Grinsven, H. J. M. V., Abrol, Y. P., Adhya, T. K., and Billen, G.: Our Nutrient World:

926   the challenge to produce more food and energy with less pollution, 2013.

927   Tan, J., Fu, J. S., Dentener, F., Sun, J., Emmons, L., Tilmes, S., Sudo, K., Flemming,

928   J., Jonson, J. E., and Gravel, S.: Multi-model study of HTAP II on sulfur and nitrogen

929   deposition, Atmos. Chem. Phys., 18, 1-36, 2018.

930   Van Damme, M., Clarisse, L., Dammers, E., Liu, X., Nowak, J., Clerbaux, C.,

931   Flechard, C., Galy-Lacaux, C., Xu, W., and Neuman, J.: Towards validation of

932   ammonia (NH_3) measurements from the IASI satellite, Atmospheric Measurement

933   Techniques, 7, 12125-12172, 2014a.

934   Van Damme, M., Wichink Kruit, R., Schaap, M., Clarisse, L., Clerbaux, C., Coheur, P.

Atmospheric
Chemistry
and Physics
Discussions

Open Access

EGU

935   F., Dammers, E., Dolman, A., and Erisman, J.: Evaluating 4 years of atmospheric

936   ammonia (NH$_3$) over Europe using IASI satellite observations and LOTOS-EUROS

937   model results, J. Geophys. Res-Atmos., 119, 9549-9566, 2014b.

938   Van der Graaf, S. C., Dammers, E., Schaap, M., and Erisman, J. W.: Technical note:

939   How are NH$_3$ dry deposition estimates affected by combining the LOTOS-EUROS

940   model with IASI-NH$_3$ satellite observations?, Atmos. Chem. Phys., 18, 13173-13196,

941   10.5194/acp-18-13173-2018, 2018.

942   Vet, R., Artz, R. S., Carou, S., Shaw, M., Ro, C.-U., Aas, W., Baker, A., Bowersox, V.

943   C., Dentener, F., Galy-Lacaux, C., Hou, A., Pienaar, J. J., Gillett, R., Forti, M. C.,

944   Gromov, S., Hara, H., Khodzher, T., Mahowald, N. M., Nickovic, S., Rao, P. S. P., and

945   Reid, N. W.: A global assessment of precipitation chemistry and deposition of sulfur,

946   nitrogen, sea salt, base cations, organic acids, acidity and pH, and phosphorus, Atmos.

947   Environ., 93, 3-100, http://dx.doi.org/10.1016/j.atmosenv.2013.10.060, 2014.

948   Vitousek, P. M., Aber, J. D., Howarth, R. W., Likens, G. E., Matson, P. A., Schindler,

949   D. W., Schlesinger, W. H., and Tilman, D. G.: Human alteration of the global nitrogen

950   cycle: sources and consequences, Ecol. Appl., 7, 737-750, 1997.

951   Wesely, M., and Hicks, B.: Some factors that affect the deposition rates of sulfur

952   dioxide and similar gases on vegetation, Journal of the Air Pollution Control

953   Association, 27, 1110-1116, 1977.

954   Whitburn, S., Van Damme, M., Clarisse, L., Bauduin, S., Heald, C. L., Hadji-Lazaro,

955   J., Hurtmans, D., Zondlo, M. A., Clerbaux, C., and Coheur, P. F.: A flexible and robust

956   neural network IASI-NH$_3$ retrieval algorithm, J. Geophys. Res-Atmos., 121,

957   6581-6599, 10.1002/2016JD024828, 2016.

958   Williams, J. E., Boersma, K. F., Le Sager, P., and Verstraeten, W. W.: The

959   high-resolution version of TM5-MP for optimized satellite retrievals: description and

960   validation, Geosci. Model Dev., 10, 721-750, 10.5194/gmd-10-721-2017, 2017.

961   Wong, D. C., Pleim, J., Mathur, R., Binkowski, F., Otte, T., Gilliam, R., Pouliot, G.,

962   Xiu, A., Young, J. O., and Kang, D.: WRF-CMAQ two-way coupled system with

963   aerosol feedback: software development and preliminary results, Geosci. Model Dev.,

964   5, 299-312, 10.5194/gmd-5-299-2012, 2012.

965   Xu, W., Luo, X. S., Pan, Y. P., Zhang, L., Tang, A. H., Shen, J. L., Zhang, Y., Li, K. H.,

966   Wu, Q. H., Yang, D. W., Zhang, Y. Y., Xue, J., Li, W. Q., Li, Q. Q., Tang, L., Lv, S. H.,

967   Liang, T., Tong, Y. A., Liu, P., Zhang, Q., Xiong, Z. Q., Shi, X. J., Wu, L. H., Shi, W.

968   Q., Tian, K., Zhong, X. H., Shi, K., Tang, Q. Y., Zhang, L. J., Huang, J. L., He, C. E.,

969   Kuang, F. H., Zhu, B., Liu, H., Jin, X., Xin, Y. J., SHi, X. K., Du, E. Z., Dore, A. J.,

970   Tang, S., Collett Jr, J. L., Goulding, K., Sun, Y. X., Ren, J., Zhang, F. S., and Liu, X. J.:

971   Quantifying atmospheric nitrogen deposition through a nationwide monitoring

972   network across China, Atmos. Chem. Phys., 15, 12345-12360, 2015.

973   Yu, G., Jia, Y., He, N., Zhu, J., Chen, Z., Wang, Q., Piao, S., Liu, X., He, H., Guo, X.,

974   Wen, Z., Li, P., Ding, G., and Goulding, K.: Stabilization of atmospheric nitrogen

975   deposition in China over the past decade, Nat. Geosci., 12, 424-429,

976   10.1038/s41561-019-0352-4, 2019.

977   Zhang, L., Wright, L. P., and Asman, W. A. H.: Bi-directional air-surface exchange of

978   atmospheric ammonia: A review of measurements and a development of a big-leaf

979 model for applications in regional-scale air-quality models, J. Geophys. Res-Atmos.,

980 115, 898-907, 2010.

981 Zhang, L., Jacob, D. J., Knipping, E. M., Kumar, N., Munger, J. W., Carouge, C., Van

982 Donkelaar, A., Wang, Y., and Chen, D.: Nitrogen deposition to the United States:

983 distribution, sources, and processes, Atmos. Chem. Phys., 12 4539-4554, 2012.

984 Zhang, Q., Streets, D. G., Carmichael, G. R., He, K., Huo, H., Kannari, A., Klimont,

985 Z., Park, I., Reddy, S., and Fu, J.: Asian emissions in 2006 for the NASA INTEX-B

986 mission, Atmos. Chem. Phys., 9, 5131-5153, 2009.

987 Zhang, X. Y., Lu, X. H., Liu, L., Chen, D. M., Zhang, X. M., Liu, X. J., and Zhang, Y.:

988 Dry deposition of NO_2 over China inferred from OMI columnar NO_2 and atmospheric

989 chemistry transport model, Atmos. Environ., 169, 2017.

990 Zhang, X. Y., Chuai, X. W., Liu, L., Zhang, W. T., Lu, X. H., Zhao, L. M., and Chen,

991 D. M.: Decadal Trends in Wet Sulfur Deposition in China Estimated From OMI SO_2

992 Columns, J. Geophys. Res-Atmos., 123, 10796-10811, 10.1029/2018JD028770, 2018.

993 Zhao, X., Chen, L., and Zhang, H.: Nitrate and ammonia contaminations in drinking

994 water and the affecting factors in Hailun, northeast China, Journal of Environmental

995 Health, 75, 28, 2013.

996 Zhao, Y., Zhang, L., Chen, Y., Liu, X., Xu, W., Pan, Y., and Duan, L.: Atmospheric

997 nitrogen deposition to China: A model analysis on nitrogen budget and critical load

998 exceedance,   Atmos.   Environ.,   153,   32-40,

999 http://dx.doi.org/10.1016/j.atmosenv.2017.01.018, 2017.

1000